IEEE Access
Multidisciplinary ⋮ Rapid Review ⋮ Open Access Journal

Received August 2, 2021, accepted August 17, 2021, date of publication August 18, 2021, date of current version August 26, 2021.

Digital Object Identifier 10.1109/ACCESS.2021.3106236

Dynamic Stability Improvement of Power System by Means of STATCOM With Virtual Inertia

LAVR VETOSHKIN, (Member, IEEE), AND ZDENĚK MÜLLER, (Senior Member, IEEE)
Department of Electrical Power Engineering, Czech Technical University, 166 36 Prague, Czech Republic

Corresponding author: Lavr Vetoshkin (vetoslav@fel.cvut.cz)

This work was supported by Czech Technical University, Prague, under Grant SGS20/165/OHK3/3T/13.

ABSTRACT The paper investigates the application of Static Synchronous Compensator (STATCOM) with synchronverter control to enhance dynamic stability. Synchronverter is a control strategy for voltage source converters that emulates a synchronous generator, therefore providing virtual inertia. A thorough analysis of system stability with STATCOM controlled using synchronverter is presented. Furthermore, a comparison to vector control is provided. The analysis was conducted for a commonly known Single Machine Infinite Bus (SMIB) test case. The authors also compare the synchronverter and vector control performance using different mathematical tools such as eigenvalue analysis, numerical simulation, and lyapunov theory. Synchronverter algorithm improves the damping of the system, as small-signal analysis shows. The results of numerical simulations demonstrate the improvement of dynamic stability. Besides, the stability region also improves in the case of synchronverter. Finally, the paper demonstrates on the IEEE 39 bus system that the operation of STATCOM with a synchronverter control strategy is feasible and improves dynamic stability. Synchronverter brings the advantages of artificially adding inertia to the system, an essential issue in modern power systems.

INDEX TERMS Power system stability, virtual inertia, virtual synchronous generator, synchronverter, STATCOM, small-signal stability, region of attraction.

NOMENCLATURE

ABBREVIATIONS AND SYMBOLS

AC	Alternating Current.
DC	Direct Current.
IEEE	Institute of Electrical and Electronics Engineers.
PCC	Point of Common Coupling.
PLL	Phase Locked Loop.
PS	Power System.
RES	Renewable Energy Source.
ROCOF	Rate of Change of Frequency.
SG	Synchrnous Generator.
SMIB	Single Machine Infinate Bus.
STATCOM	Static Synchronous Compensator.
UPFC	Unified Power Flow Controller.
VSC	Voltage Scource Converter.
VSG	Virtual Synchronous Generator.
Δx	State vector.
ζ	Damping ratio.
λ	Eigenvalue.
$\mathbf{A}$, $\mathbf{B}$	State/Input matrix.
C_{dc}	STATCOM DC capacitance.
D	Droop.
J	Inertia Constant.
$K_{p,dc}$,$K_{i,dc}$	PI Gain of DC voltage controller.
$K_{i,p}$, $K_{i,i}$	PI gains of current controller.
$K_{i,v}$	Gain of intergral voltage controller.
$\mathbf{m_d}$, $\mathbf{m_q}$	Modulation signal in $d-q$ axis.
v_d, v_q	Node voltage in $d-q$ axis.
L_f, R_f	Filter inductance and resistance.
P_{el}	Active electrical power.
P_{mech}	Mechanical power.
pu	Per Unit.
T_e	Electric troque.
V_{KE}, V_{PE}	Kinetic/Potential Energy.
x	Reactance.
y	Admitance.

STATE VARIABLES

δ	Load angle.
ψ_f	Virtual excitation flux.

The associate editor coordinating the review of this manuscript and approving it for publication was Qiuhua Huang.

ω	Angular velocity.
i_d, i_q	Current in $d-q$ axis.
$i_{d,ref}$	State variable of active power controller.
$i_{q,ref}$	State variable of voltage in PCC controller.
v_{dc}	Voltage of DC capacitor.
$p_{reg,pi}$	DC voltage controller state variable.
M_d, M_q	State variable of $d-q$ current controllers.

I. INTRODUCTION

Nowadays, people demand from companies to be more sustainable and reduce their carbon footprint. The electric power industry is under pressure to phase out conventional power plants, especially coal, and increase the share of renewables in their energy mix. This trend changes the traditional ways of power system control. With a larger share of renewables, the overall system inertia has decreased. Nevertheless, nuclear power plants have broad support from many people since they can be considered carbon neutral. Thus, synchronous generators are here to stay, at least for the foreseeable future. However, the industry has to learn how to operate synchronous generators in a system with a larger share of solar and wind that does not utilize SGs with large inertia. Different control methods and power electronics can be utilized to ensure the stability of the grid. Flexible AC transmission system (FACTS) devices have become a more common solution for modern power systems, especially with the reduction of power electronic components costs.

Researchers propose control strategies for power converters that can emulate inertia response to cope with the changing grid dynamics, thus substituting Synchronous Generator's (SG) inertia. Those strategies are commonly known as Virtual Synchronous Generators (VSG) [1]–[3]. A VSG emulates synchronous generator behavior, i.e., providing virtual inertia. Many researchers divide VSGs into two categories grid-following, and grid-forming [4]. The grid-forming approach has the benefit of not requiring Phase Locked Loop (PLL) for synchronization, which in many cases improves the stability of the system [5]. Furthermore, grid-forming VSG usually utilizes swing equation to emulate SG, whereas grid-following can be built on top of vector control [6]. Such algorithms can be called Rate of Change of Frequency VSG [5]. However, this approach has similar stability weaknesses as vector control due to PLL, though providing inertia [5]. Another approach that is fairly broadly used is droop control. Paper [7] compares this grid-following control strategy to emulation of inertia. The results provided in the paper [7] suggest that a VSG has an advantage over pure droop control. Furthermore, from a frequency control, perspective droop control can be classified as the proportional term and inertia as the derivative term of control. Therefore, it is better to utilize both virtual inertia and droop control altogether [8].

Typically, STATCOMs are controlled using vector control and can provide reactive power or voltage control in Point of Common Coupling (PCC). Furthermore, STATCOMs with relatively large capacitors can provide short-term active power support [9]. Logically, the STATCOM has very similar characteristics to photovoltaic power plants connected to the grid via VSC. It makes it a good candidate to explore the possibility of the application of virtual inertia control to STATCOM to enhance power system stability. In the paper [10] such system is referred to as Virtual Synchronous Compensator (VSCOM). This approach to the control of STATCOM brings benefits of providing short-term frequency control during transients without losing the ability to control/reactive power in the node during normal operation. STATCOMS to the contrary of photovoltaic/wind power plants do not require extensive land use. Thus, it essentially can be put in any node of the PS and provide virtual inertia. The placement of virtual inertia was shown to be an important parameter in the system [5], [11]. Paper [10] outlines that VSCOM is more stable than traditional control, especially in weak grids. Some researchers studied the application of STATCOM with battery energy storage. For example, [12] proposes vector control with droop regulation to support grid frequency. Furthermore, paper [13] examines the application of virtual inertia to UPFC with battery. Nevertheless, the authors point out that UPFC is a very costly solution even comparing to STATCOMs. FACTS manufacturers seem to bet on further development and expansion of the STATCOM market in Europe. Series type and combined compensators are a relatively small percentage of FACTS [14], [15], and STATCOMs slowly replace SVCs.

As previously mentioned in this paper, the synchronverter is applied to STATCOM to introduce virtual inertia in the system. Synchronverter is a grid-forming control strategy that utilizes swing equation to emulate SG [2]. Since it employs the second-order model of SG, it provides virtual inertia advantages without algorithmic complexity compared to higher-order models. The paper presents the comparison of the system's stability with the classic vector control of STATCOM with the synchronverter. Section II describes mathematical models of the system in $d-q$ reference frame. In the next section, the stability of the Single Machine Infinite Bus (SMIB) system is analyzed. The authors chose the following methods for analysis small-signal stability, estimation of regions of attractions using Lyapunov's method, and numerical simulations. Simplified models gave a reasonable estimation of regions of attraction for both cases. The results were then verified using numerical simulations. Furthermore, the authors compare the stability using the commonly known IEEE 39 bus benchmark system. The results are then discussed in conclusion.

II. SYSTEM MODEL

This section provides explanations and modeling assumptions for the test case model in $d-q$ reference frame. The discussed nonlinear models of STATCOM with both compared control strategies were implemented in Wolfram Mathematica [16]. For the SMIB case, the authors chose to use 7^{th} order model, which is fairly complex and better

approximates the dynamics of a SG. The same model is used, for example, in SimScapePower Systems. More on the modeling of the synchronous machine can be found in [17]–[19]. The assumptions that were used to compile the model of the system using differential-algebraic equations are explained in [[5], Sec. 2.6].

A. STATCOM MODEL

STATCOM is a VSC connected to the grid through a transformer, with the DC side being only energy storage. Fig. 1 shows the schematic diagram of the VSC with an L-type filter. In $d-q$ reference frame, the equations describing the dynamics of this subsystem are the following:

$$\frac{\mathbf{m_d} v_{dc}}{2} = L_f \frac{\mathrm{d}i_d}{\mathrm{d}t} - \omega_s L_f i_q + R_f i_d + v_d \tag{1}$$

$$\frac{\mathbf{m_q} v_{dc}}{2} = L_f \frac{\mathrm{d}i_q}{\mathrm{d}t} + \omega_s L_f i_d + R_f i_q + v_q \tag{2}$$

where L_f is filter inductance and R_f is resistance. $\mathbf{m_q}$ is power electronics modulation of the imaginary part of the voltage vector, which is provided by the control algorithm.

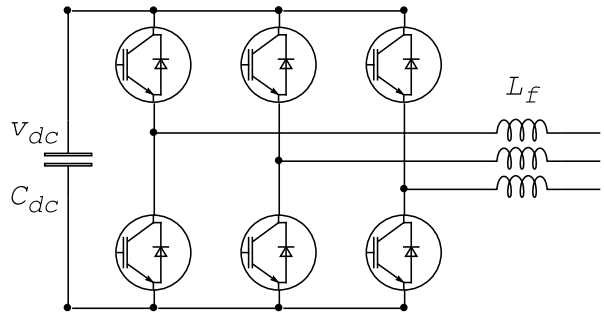

FIGURE 1. VSC schematic diagram. Adopted from [5].

Usually, in the modeling of power converters, the DC side and switching losses are neglected. Thus the dynamics of the DC voltage can be described as follows:

$$C_{dc} \frac{\mathrm{d}v_{dc}}{\mathrm{d}t} = \frac{-p_{vsc}}{v_{dc}} \tag{3}$$

where C_{dc} is DC capacitor and p_{vsc} is power exchange with the grid. For the average model, power exchange between grid and VSC can be computed using the following formula:

$$p_{vsc} = (\mathbf{m_d} v_{dc} i_d + \mathbf{m_q} v_{dc} i_q)/2 \tag{4}$$

B. SYNCHRONVERTER MODEL IN D – Q REFERENCE FRAME

Fig. 2 shows the block diagram of the synchronverter. The current and voltage measurements are required for subsequent calculations of virtual torque, reactive power, and voltage reference. The torque is computed using the current vector multiplied by sinusoids that use virtual mechanical angle (θ) and virtual magnetic flux ($M_f i_f$) (eq. (5)). Note, reactive power is directly controlled through the flux without considering the dynamics of the excitation winding. The reactive power is computed using eq. (7). The voltage reference

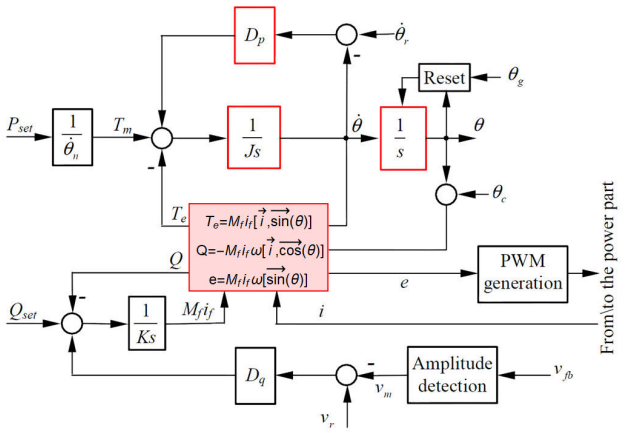

FIGURE 2. Synchronverter block diagram. Adapted from [2].

(eq. (6)) for PWM is calculated using the virtual magnetic flux and machine angle.

$$T_e = M_f i_f[\vec{i}, \vec{sin}(\theta)] \tag{5}$$

$$e = \dot{\theta} M_f i_f \vec{sin}(\theta) \tag{6}$$

$$Q = -\dot{\theta} M_f i_f[\vec{i}, \vec{\cos}(\theta)] \tag{7}$$

where $\vec{i} = \begin{bmatrix} i_a \\ i_b \\ i_c \end{bmatrix}$ and $\vec{\sin}(\theta) = \begin{bmatrix} sin(\theta) \\ sin(\theta + \frac{2\pi}{3}) \\ sin(\theta - \frac{2\pi}{3}) \end{bmatrix}$

Furthermore, the synchronverter utilizes droop control for frequency regulation. Hence, it is considered a grid-forming device in the system [4]. However, the power injection to support frequency can be short since the DC capacitor relative to inertia stores a small amount of energy, and photovoltaic or wind power plants can hardly increase power production on demand.

The synchronverter from the grid perspective should mimic the behavior of a SG [2]. The equations in the previous subsection described the dynamics of the electric part of the subsystem II-A. This part is essentially concerned with modulations signal $\mathbf{m_d}$ and $\mathbf{m_q}$ and incorporation of this subsystem to the network. In the synchronverter, there is no magnetic coupling from the stator to the rotor. Hence, there is only one coupling from virtual excitation to the stator in the model, that emulates emf. Thus $v_{d,synch} = 0$ and $v_{q,synch} = \omega_r \psi_f$, where ω_r is virtual angular velocity and ψ_f is virtual excitation flux [23]. Hence, the modulation signals for synchronverter in eq. (1) and (2) become $\mathbf{m_d} = 0$ and

$$\mathbf{m_q} = \omega_r \psi_f \tag{8}$$

Note, that the eq. (1) and (2) then are defined for the synchronverter rotating frame, thus grid voltages should be transformed accordingly.

As explained in [5], the vectors can be transformed from one frame to another using [[5], eq. (41)]. The equation

linking rotating frames is as follows:

$$\frac{\mathrm{d}\delta}{\mathrm{d}t} = \omega_r - \omega_s \tag{9}$$

The swing equation that computes the virtual angular velocity:

$$J\frac{\mathrm{d}\omega_r}{\mathrm{d}t} = \frac{p_{mech}}{\omega_s} - \frac{p_{synch}}{\omega_s} - D_p(\omega_r - \omega_s) \tag{10}$$

where power injected by synchronverter p_{synch} in rotating reference frame is calculated considering assumptions eq. (4) and (8). Thus,

$$p_{synch} = \frac{\omega_r \psi_f v_{dc}}{2} i_q^r \tag{11}$$

In eq. (10) p_{mech} is virtual mechanical power input, which is used to control DC voltage. Hence, for PI controller with $K_{p,dc}$ and $K_{i,dc}$ that are proportional and integral constants respectively the following equations are valid:

$$p_{mech} = K_{p,dc}(v_{dc} - v_{dc,ref}) + p_{reg,pi} \tag{12}$$

$$\frac{\mathrm{d}p_{reg,pi}}{\mathrm{d}t} = K_{i,dc}(v_{dc} - v_{dc,ref}) \tag{13}$$

In synchronverter voltage or reactive power injection in PCC is controlled using excitation flux ψ_f [23]. In this case, the authors assumed the former for STATCOM. Thus,

$$\frac{\mathrm{d}\psi_f}{\mathrm{d}t} = K_{i,v}(v_{ref} - v_{pcc}) \tag{14}$$

where v_{pcc} is the voltage amplitude in PCC and $K_{i,v}$ is integral constant of voltage regulator.

C. VECTOR CONTROL OF STATCOM

The vector control became a standard control strategy for VSCs. This section is concerned with the vector control model in $d-q$ and how modulation signals are computed in vector control. The model neglects the effects of PLL. The objective of the control in the case of STATCOM is to maintain voltage levels in PCC and simultaneously of the capacitor. The DC voltage is controlled through the real part of the injected current vector and voltage through the imaginary part of it. Hereafter the authors just state the equations since the algorithm is fairly known in the industry (more on the modeling can be found in [9] and [25]).

$$\mathbf{m_d} = v_d - \omega_s L_f i_q + K_{p,i_d}(i_{d,ref} - i_d) + M_d \tag{15}$$

$$\mathbf{m_q} = v_q + \omega_s L_f i_q + K_{p,i_q}(i_{q,ref} - i_q) + M_q \tag{16}$$

$$\frac{\mathrm{d}M_d}{\mathrm{d}t} = K_{i,i_d}(i_{d,ref} - i_d) \tag{17}$$

$$\frac{\mathrm{d}M_q}{\mathrm{d}t} = K_{i,i_q}(i_{q,ref} - i_q) \tag{18}$$

$$\frac{\mathrm{d}p_{reg,pi}}{\mathrm{d}t} = K_{i,dc}(v_{dc} - v_{dc,ref}) \tag{19}$$

$$\frac{\mathrm{d}i_{d,ref}}{\mathrm{d}t} = K_{i,p}(p_{reg,pi} + K_{p,dc}(v_{dc} - v_{dc,ref}) - p_{vsc}) \tag{20}$$

$$\frac{\mathrm{d}i_{q,ref}}{\mathrm{d}t} = K_{i,v}(v_{ref} - v_{pcc}) \tag{21}$$

K_{p,i_d} equals K_{p,i_q} and K_{i,i_d} equals K_{i,i_q} since current controllers though decoupled use same parameters

III. STABILITY COMPARISON

This section investigates the stability of the system with STATCOM using synchronverter control. Furthermore, a comparison to vector control is provided. The authors chose to take a commonly known case of a SMIB system with a STATCOM. For the system, the small-signal stability analysis was conducted, and the region of attraction was estimated for both control strategies. Furthermore, numerical simulations were run to verify the validity of estimations of stability regions. Lastly, the conclusions are verified in the IEEE 39 bus test system.

A. SYSTEM DESCRIPTION

Fig. 3 shows a line diagram of the system that authors used for further analysis. The generator's parameters are shown in the Appendix I. STATCOM, in the case of both algorithms, controls the voltage level in the second node. The STATCOM in the model has parameters in the Appendix II. Furthermore, the admittance matrix 4 by 4 describes the network and can be assumed from Fig. 3.

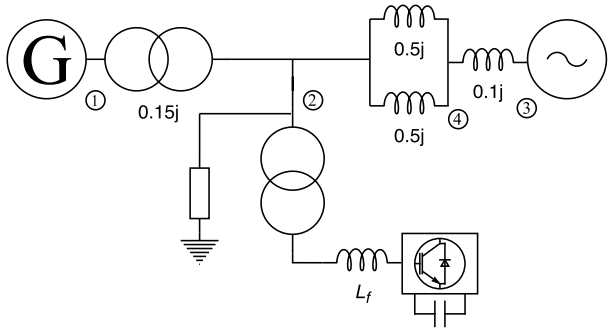

FIGURE 3. Line diagram of the system.

B. SMALL-SIGNAL STABILITY

Small-signal stability analysis is a commonly used tool for stability studies that provides information about system behavior without solving the equations. However, it has some limitations since the results are valid for small disturbances. As previously mentioned, the model is described by the system of differential equations and a system of linear algebraic equations. To examine the stability of the system using eigenvalues, firstly, the model should be simplified to the system of differential equations and then linearized around the operating point using first-order Taylor expansion. The linearized model can be generally described by eq. (22) which is basically a state-space representation of a linear system

$$\Delta\dot{x} = \mathbf{A} \cdot \Delta x + \mathbf{B} \cdot u \tag{22}$$

where $\mathbf{A}$ is state or system matrix and $\mathbf{B}$ is input matrix. State vector Δx consist of seven variables of synchronous generator with parameters in Appedix A and states of synchronverter control that can be found in equations in section II-B (eq. (9),(10),(13),(14)). Also, to the state variables should be

added three states of VSC model that can be found in II-A. In the small-signal analysis, the concern is the state matrix's eigenvalues $\mathbf{A}$, which show if the system converges. It can be shown by solving the general form of equations that for $Re(\lambda) > 0$ solution in $t \to \infty$ does not converge. By following the steps above, the authors computed the eigenvalues of the system for both control algorithms. Tab. 1 shows the computed eigenvalues for both control strategies and minimum damping ratios as well.

TABLE 1. Computed eigenvalues of the system with different control strategies.

Control algorithm	Eigenvalues	Min ζ
Synchronverter	$-298.122 \pm 2961.75j$, $\mathbf{-74.0969 \pm 1014.53j}$, $-96.4019 \pm 258.276j$, $-2.25383 \pm 8.60414j$, $-0.93304 \pm 7.20548j$, $-6.29137, -3.66956$, $-0.0725057 \pm 0.0357883j$	0.07284
Vector control	$-61.2246 \pm 1341.88j$, $-11.2496 \pm 864.238j$, $-11.8959 \pm 10.7522j$, $-0.700878 \pm 9.55667j$, $-6.29137, -3.30489$, $\mathbf{-0.00686874 \pm 1.18525j}$, $-0.119065 \pm 0.0612463j$, $-0.00749973 + 0j$	0.005795

Further insight into the stability of the system can be gained by analyzing the difference in eigenvalues placement for different control strategies. Fig. 4 show that in the case of synchronverter, eigenvalues have been pushed to the left. Additionally, the damping ratio ζ of the eigenvalues can be analyzed as well. If we assume that eigenvalue is defined as $\lambda = \sigma + j\omega$ then the damping ratio is as follows:

$$\zeta = \frac{\sigma}{\sqrt{\sigma^2 + \omega^2}} \tag{23}$$

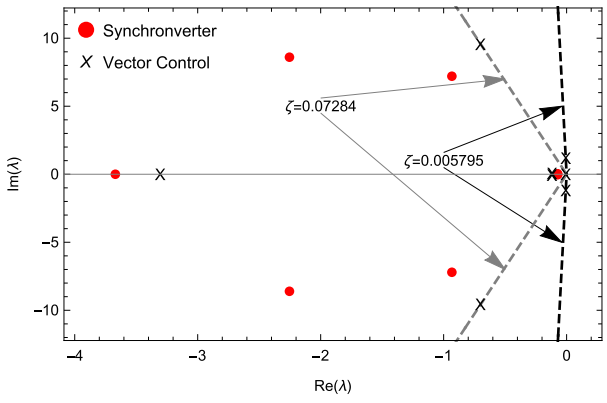

FIGURE 4. Eigenvalues of the system with different control algorithms of STATCOM.

Tab. 1 show the minimum damping ratio, and the corresponding eigenvalues are highlighted. Furthermore, in Fig. 4 the dashed lines show the set of points corresponding to both cases' minimum damping ratios. Consequently, any eigenvalue that lies between the x-axis and the dashed line has a higher damping ratio. The results of calculations show that the system response to disturbances can be improved by introducing synchronverter control.

C. NUMERICAL SIMULATIONS

1) LOAD CHANGE

The load change test is a typical transient stability study that authors consider in the paper. A sudden change in load in the system can produce oscillations, which then, if the controllers are tuned incorrectly, might lead to instability. Furthermore, this test will demonstrate the stability of the examined approaches to damp oscillations. From the previous section, one can conclude that the STATCOM with synchronverter control would improve the system's performance. The authors of the test chose the following scenario. In simulation time $t = 5s$, in node 2, the load suddenly increases by 30 MW.

It is clear from Fig. 5 that STATCOM with synchronverter damps oscillations caused by load increase faster. However, the voltage deviation from the reference is more significant. However, the STATCOM with vector control allows a higher deviation of generator velocity and provides lower damping. Further, analysis of such disturbance can be conducted by quantifying the quality of the control with different criteria. Most commonly used are integral of the absolute value of the error and integral of the squared absolute value of the error. The first criterium shows the area of error during a transient. However, the second criterium penalizes the greater deviations from the reference point. Tab. 2 shows results of simulation for different load increases. The conclusion from the computed values of criteria is clear that synchronverter control is faster in every case because it damps oscillations faster. Hence the total area of error is smaller. However,

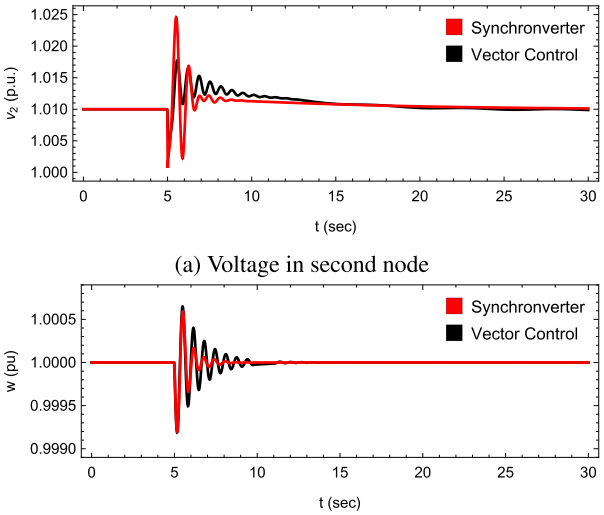

(a) Voltage in second node

(b) Angular velocity of the generator

FIGURE 5. Load increase in $t = 5s$ by 30MW.

TABLE 2. Load test: quality of control.

Control algorithm	Load change	$\int \lvert v_2 - v_{ref}\rvert \mathrm{d}t$	$\int \lvert v_2 - v_{ref}\rvert^2 \mathrm{d}t$
Synchronverter	$30MW$	$24.928 * 10^{-3}$	$92.216 * 10^{-6}$
	$45MW$	$35.979 * 10^{-3}$	$197.525 * 10^{-6}$
	$60MW$	$46.129 * 10^{-3}$	$334.415 * 10^{-6}$
Vector control	$30MW$	$28.039 * 10^{-3}$	$79.091 * 10^{-6}$
	$45MW$	$40.405 * 10^{-3}$	$165.057 * 10^{-6}$
	$60MW$	$51.669 * 10^{-3}$	$271.667 * 10^{-6}$

the second criterium of control quality says that the synchronverter algorithm allows higher voltage deviation than vector control. If one considers only how fast the voltage reference value is restored in the node, the synchronverter is the better choice. Furthermore, if rotor speed deviation is of greater concern, the vector control is not preferable since it has worse performance, as Fig. 5 demonstrates.

2) THREE-PHASE FAULT TEST

Transient stability studies are always concerned with three-phase faults since it is the most severe fault that can occur in the power system. In the test case, the authors considered a fault occurring in the transmission line, and after the fault is cleared, the faulted line is disconnected. Hence, the reactance of the transmission between node 2 and node 4 increases by the factor of two. The scenario of simulation is the following: the power system before disturbance occurs is in a steady-state. The fault occurs in time $-t_{cl}$ and the fault is clear in $t = 0$. Since the fault test is concerned with the system's post fault performance, the $5s$ of the post fault performance is presented in the paper. The authors chose two clearing times for the test case. Clearing time $0.1s$, which is common for such studies. However, in power systems, $t_{cl} = 0.2s$ is a more realistic clearing time that relay protection devices can assure.

Fig. 6 show the results of the simulation for a three-phase fault with $t_{cl} = 0.1s$. For both cases, the system is stable. However, a closer look shows that the maximum speed deviation is higher in cases of vector control. As previously stated, the synchronverter adds virtual inertia to the system. Hence, the overall system behaves like it has higher inertia. That explains the system's better performance in terms of lower speed and load angle deviation from steady value. Furthermore, the damping of the oscillations is also improved in the case of synchronverter (Fig. 6), even though it is in the system with lower inertia easier to damp oscillations.

Fig. 7 shows that in case of $t_{cl} = 0.2s$, the system with vector control is unstable. It is clear that by adding virtual inertia, transient stability is greatly improved because the generator does not speed up to a point where it cannot swing back and lose synchronism. Furthermore, after the disturbance, the oscillations are damp during the first 5 post fault seconds.

D. REGION OF ATTRACTION

This section provides the estimation of the region of attraction for both cases and compares the results. The authors used simplified models of devices for computation. Nevertheless,

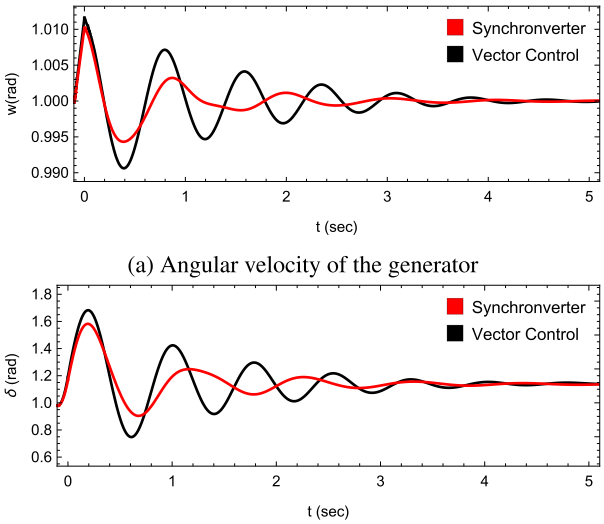

(a) Angular velocity of the generator

(b) Load angle of the generator

FIGURE 6. Three-phase short circuit simulation results for $t_{cl} = 0.1s$.

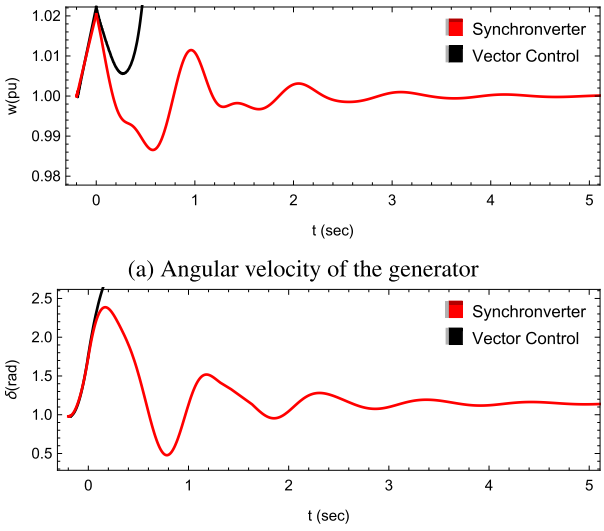

(a) Angular velocity of the generator

(b) Load angle of the generator

FIGURE 7. Three-phase short circuit simulation results for $t_{cl} = 0.2s$.

the yielded results are quite accurate as numerical simulations showed.

1) ESTIMATION FOR VECTOR CONTROL

To estimate the region of attraction of the system with vector control, applied a simplified model of a SG and the STATCOM with vector control. Fig. 8 shows the equivalent circuit of the analyzed system. For the estimation of the region of attraction, firstly, the system model should be stated hereafter. The second-order model of the machine is often used for such analysis.

$$\delta_g = \Delta\omega \tag{24}$$

$$J\frac{\mathrm{d}\omega}{\mathrm{d}t} = P_{mech} - P_{el} - D\Delta\omega \tag{25}$$

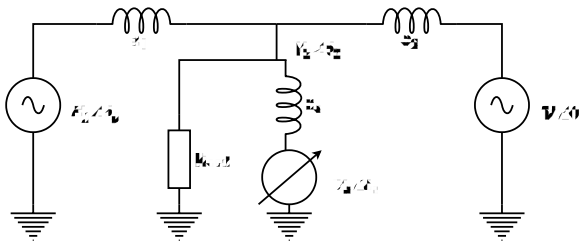

FIGURE 8. The equivalent circuit of the system with STATCOM.

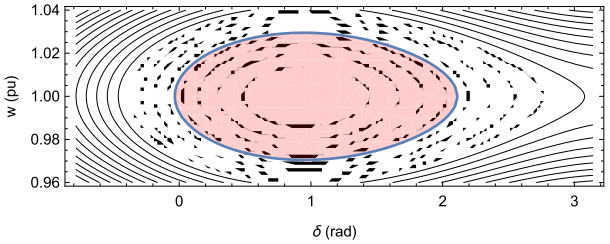

FIGURE 9. Contour plot of the Lyapunov function and region of attraction. (System with vector control).

The power produced by the electromagnetic forces in the generator can be assumed from 8:

$$I_g = \frac{E_g e^{j\delta_g} - V_2 e^{j\delta_2}}{jx_1} \tag{26}$$

$$P_{el} = Re(E_g e^{j\delta_g} I_g^*) \tag{27}$$

However, the voltage in node two should be written in terms of STATCOM voltage and grid voltage as in [26] The current injection by STATCOM can be calculated as follows:

$$I_s = \frac{V_s e^{j\delta_s} - V_2 e^{j\delta_2}}{jx_s} \tag{28}$$

where $x_s = \omega L_f + \omega L_t$ reactance is a sum of filter and a transformer reactances.

The current flowing into the grid:

$$I_{grid} = \frac{V_2 e^{j\delta_2} - V}{jx_2} \tag{29}$$

Thus, the current Kirchhoff law for the node 2 is:

$$I_g + I_s + I_{grid} + y_{load} V_2 e^{j\delta_2} = 0 \tag{30}$$

where y_{load} is load admittance.

By solving eq. (28) - (30) the voltage in second node can be obtained in terms of voltage of STATCOM and grid voltage. Then in eq. (27) the V_2 can be substituted, and the formula for power injected by generator obtained.

After that, the Lyapunov function can be defined as follows:

$$V(\omega, \delta_g) = \frac{1}{2} J \Delta\omega^2 + \int_{\delta_g(0)}^{\delta_g} (-P_{mech} + P_{el} + D\Delta\omega) \mathrm{d}\delta_g \tag{31}$$

And critical value of the function is calculated as in [18]

$$V_{critical} = \int_{\delta_g(0)}^{\pi - \delta_g(0)} (-P_{mech} + P_{el}) \mathrm{d}\delta_g \tag{32}$$

Fig. 9 shows the region of attraction of the system where $V(\omega, \delta_g) < V_{critical}$. Hence, every solution of the system with initial condition inside the bounded region will converge in $t \to \infty$ to some stable state $(\delta_{g,stable}, \omega_{stable})$

2) ESTIMATION FOR SYNCHRONVERTER

To estimate the region of stability of the system with STATCOM controlled as a synchronverter, the authors assume that the STATCOM during transient can be viewed as a synchronous machine with inertia that equals to virtual inertia and mechanical power input zero. Hence, the systems become a multimachine system where two machines are connected to the infinite bus. For such cases, a number of proven methods for the estimation of critical energy and regions of stability exist. The authors chose to use Potential Energy Boundary Surface (PEBS) method that is explained, for example, in [17]. This method is basically an extension of the SMIB critical energy calculation for a multimachine system. Thus, it uses the simplified model of the generator. Thus, the following equations describe the dynamic system:

$$J \frac{\mathrm{d}\omega_i}{\mathrm{d}t} = P_{mech,i} - P_{el,i} - D\Delta\omega_i \tag{33}$$

$$\delta_{g,i} = \Delta\omega_i \tag{34}$$

It should be mentioned that the network admittance matrix also changes since the estimation is done for the post fault system where one of the transmission lines is disconnected.

The energy function of the individual machine is as follows:

$$V_i = \frac{1}{2} J_i \Delta\omega_i^2 - \int_{\delta_{i,s}}^{\delta_i} P_{mech,i} - P_{el,i} - D\Delta\omega_i \mathrm{d}\delta_i \tag{35}$$

where $(\omega_{i,s}, \delta_{i,s})$ is stable operating point of the machine. Energy function can be presented as sum of kenetic and potential energies $V_i = V_{KE,i} + V_{PE,i}$

And the total energy function of the system is the sum of the energy functions of the devices. The estimation of the critical energy, in this case, is slightly different. By integrating the fault-on trajectory, the V_{PE}^{max} can be found, then it can be assumed to be the $V_{critical}$ [17].

Fig. 10 shows the rendering of the energy function for the generator while velocity and load angle of the second machine (synchronverter) are equal to $(\omega_{2,s}, \delta_{2,s})$ stable steady values.

3) COMPARISON

It should be reiterated that the estimation was done using the simplified model, and for the PEBS case, some assumptions could lead to inaccurate results, as explained in [21]. Let us

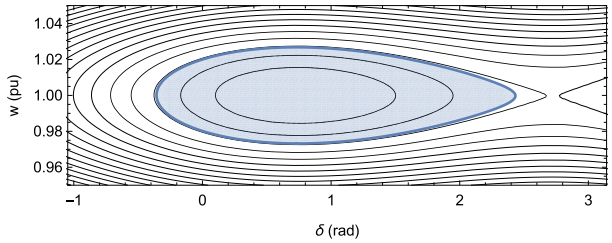

FIGURE 10. Contour plot of the Energy function and region of attraction. (System with synchronverter control).

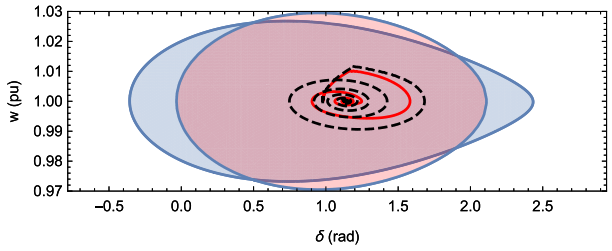

(a) Three-phase fault $t_{cl} = 0.1s$.

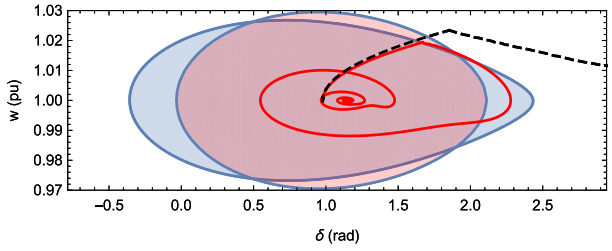

(b) Three-phase fault $t_{cl} = 0.2s$.

FIGURE 11. The region of attraction of the system with synchronverter (Blue), system with vector control (Pink) and the phase-space transient trajectories system with synchronverter (Red), system with vector control (Dashed, Black).

compare the results of the estimated stability regions. Fig. 11 shows the regions of stability and fault trajectories for both examined cases. It is clear that the region of stability in the case of synchronverter is larger. Furthermore, it is surprisingly accurate if compared to the fault trajectory in Fig. 11b. It (Fig. 11b) also shows that in the case of vector control, the trajectory leaves the stable region; hence the generator loses synchronism. However, Fig. 11b demonstrates that not the stability region in the case of synchronverter is better but the fault trajectory. Of course, the region of attraction in the case of vector control is slightly smaller but not that much. The important fact is that by adding virtual inertia, the system behaves like it, in fact, has higher inertia. Thus the generator speeds up slower. Therefore, not leaving the stable region.

4) VERIFICATION ON IEEE 39 BUS

In the previous chapter, the authors compared vector control to a synchronverter in a classic SMIB system. Such a system allows gaining insides into the dynamics of a system with the examined strategies. However, the outcome of the analysis

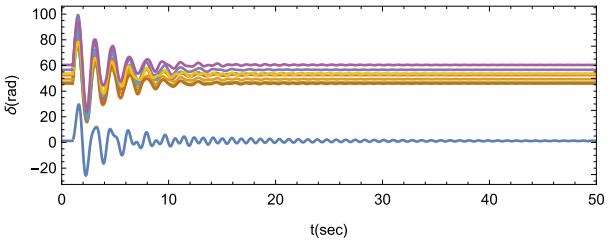

(a) Synchronverter control

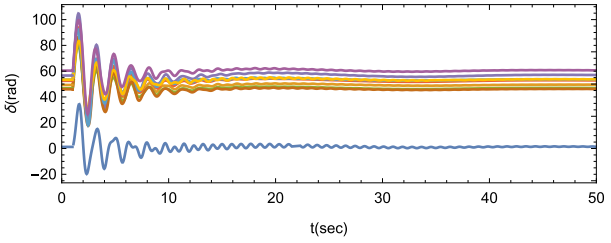

(b) Vector Control

FIGURE 12. First Case: Load angles of SGs. (three-phase short circuit with $t_{cl} = 0.1s$).

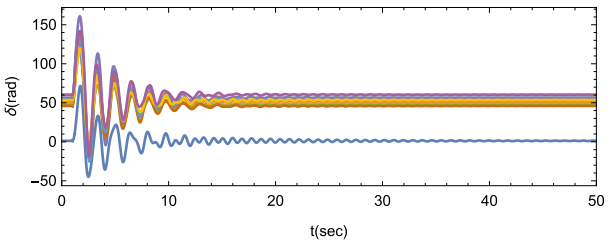

(a) Synchronverter control

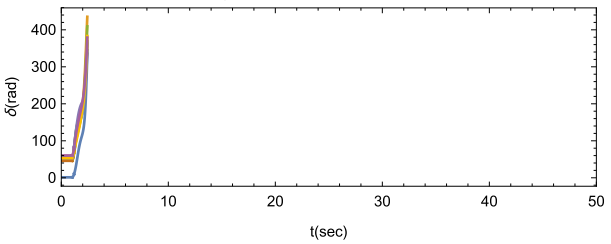

(b) Vector Control

FIGURE 13. First Case: Load angles of SGs. (three-phase short circuit with $t_{cl} = 0.2s$).

above is better to verify in a larger system. IEEE 39 bus is a common relatively complex benchmark test case, the data for the system can be found in the book by Padiyar [27]. Thus, the authors examine two cases by running simulations for both control strategies. In the first case, the VSCs are connected to nodes 14 and 18. For the second case, VSCs are connected to nodes 15 and 26. The scenario of the simulations is the following a three-phase short circuit occurs on the line between nodes 15 and 16. The authors consider the same clearing times as in SMIB cases. After the fault is cleared the line 15-16 is disconnected. The results of the simulation for the first case are presented in Fig. 12a and 13a. In that case,

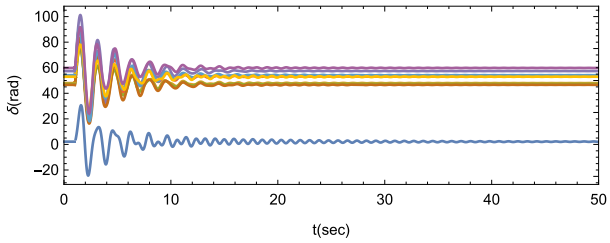

(a) Synchronverter control

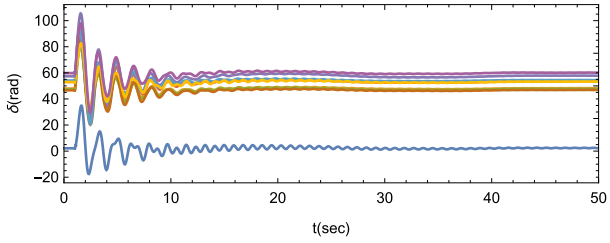

(b) Vector Control

FIGURE 14. Second Case: Load angles of SGs. (three-phase short circuit with $t_{cl} = 0.1s$).

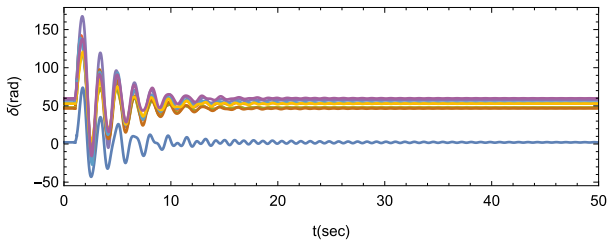

(a) Synchronverter control

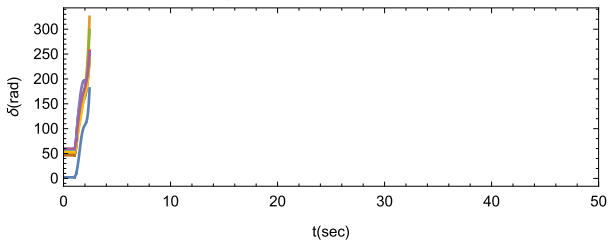

(b) Vector Control

FIGURE 15. Second Case: Load angles of SGs. (three-phase short circuit with $t_{cl} = 0.2s$).

the system with vector control cannot sustain $t_{cl} = 0.2$ and loses synchronism. The second case gives the same conclusion where the synchronverter outperforms vector control in the transient stability study.

The minimal damping ratios of individual system configurations are presented in tab. 3. The damping ratios of the examined system are not much affected by the control strategy of the VSCs. However, there is a small improvement in the case of synchronverter when connected to nodes 14 & 18. Results of simulations do not show a big difference in damping oscillations in such a large system depending on the control strategy of VSCs. Furthermore, tab. 3 includes the

TABLE 3. Performance of control strategies in IEEE 39 bus system.

	t_{cl}		14&18	14&26
Synchronverter	$0.1s$	$\min \zeta$	0.01066	0.01056
		$\max \delta$	99.3°	101.2°
		$\max \Delta f$	0.43 Hz	0.44 Hz
	$0.2s$	$\max \delta$	160.1°	167.3°
		$\max \Delta f$	0.95 Hz	0.96 Hz
Vector Control	$0.1s$	$\min \zeta$	0.00608	0.0103
		$\max \delta$	104.8°	105.6°
		$\max \Delta f$	0.45 Hz	0.45 Hz
	$0.2s$		unstable	unstable

maximum load angle deviation and frequency for different configurations of network and clearing times. The computed numbers prove the conclusions that were reached by authors in the SMIB case analysis. Synchronverter indeed increases the overall inertia in the system, thus the generators reach lower load angles during faults. Therefore, the identical system with synchronverter instead of vector control can sustain longer clearing times as simulations in Fig. 13 and 15 prove.

IV. CONCLUSION

The paper thoroughly investigates the stability of the operation of a STATCOM with a synchronverter control strategy. Furthermore, the paper compares the operation of STATCOM with vector control and synchronverter. Applying a synchronverter algorithm to the STATCOM, the dynamic stability of a generator can be enhanced. As a result, the system's damping improves and increases transient stability, especially the ability to withstand three-phase faults with a clearing time of 200 ms (Fig. 7). In addition, the paper presents numerical simulations with typical transient's stability studies such as load change and three-phase faults. The obtained results demonstrate that the overall performance of the system improves.

Moreover, the authors analyzed the region of stability of the examined SMIB system using the Lyapunov theory. To compute stability regions, the authors utilized a simplified model of the STATCOM with both control algorithms. Nevertheless, numerical simulations proved the chosen approach yielded accurate results (Fig.11). It is clear that the main improvement of stability in the case with synchronverter is it adds virtual inertia. Hence the system behaves like it has higher inertia. Thus the generator speeds up slower. Therefore even though the stability region is not much larger, the system with a synchronverter can withstand a longer clearing time. It is a very important topic in grids with high penetration of renewables that bring the challenge of low grid inertia. Consequently, STATCOM might be applied to increase the overall inertia of the system. The test case of IEEE 39 buses with two VSCs connected to different nodes confirmes that the system with synchronverter control can sustain longer clearing times.

In conclusion, the paper demonstrates that the application of a synchronverter can allow the system to withstand longer clearing times. Thus it can be applied to systems where inertia has to be increased. Besides, the pool of generators that are online in large power systems changes throughout the day, and the possible application of synchronverter can be in the management of inertia constant in intraday system control.

APPENDIX I. GENERATOR PARAMETERS

$xd = 1.3125$, $xd' = 0.1813$, $xq = 1.2578$, $xd'' = 0.16$, $xq'' = 0.25$, $Td0' = 5.89$, $Td0'' = 0.5$, $Tq0'' = 0.6$, $r_s = 0.00518$, $H = 3.01$

APPENDIX II. STATCOM PARAMETERS

VSC parameters: $S_n = 100\ MVA$, $L_f = 9.737\ mH$, $R_f = 147.4\ \mu Ohm$, $C_{dc} = 1840.5\ \mu F$, $V_{dc} = 40\ kV$

Synchronverter parameters: $J = 28.3 \cdot 10^{-3}$, $D_p = 99.5 \cdot 10^{-3}$, $K_{i,v} = 0.1$, $K_{p,dc} = 57.2 \cdot 10^{-4}$, $K_{i,dc} = 0.07$

Vector Control: $K_{i,v} = 0.31$, $K_{p,i_d} = 63.66 \cdot 10^{-4}$, $K_{i,i_d} = 12.21 \cdot 10^{-3}$, $K_{i,p} = 1.39$, $K_{p,dc} = 2.72$, $K_{i,dc} = 28.6 \cdot 10^{-3}$

REFERENCES

[1] H.-P. Beck and R. Hesse, "Virtual synchronous machine," in *Proc. 9th Int. Conf. Electr. Power Quality Utilisation*, Barcelona, Spain, Oct. 2007, pp. 1–6.

[2] Q.-C. Zhong and G. Weiss, "Synchronverters: Inverters that mimic synchronous generators," *IEEE Trans. Ind. Electron.*, vol. 58, no. 4, pp. 1259–1267, Apr. 2011, doi: 10.1109/TIE.2010.2048839.

[3] K. Shi, H. Ye, W. Song, and G. Zhou, "Virtual inertia control strategy in microgrid based on virtual synchronous generator technology," *IEEE Access*, vol. 6, pp. 27949–27957, 2018, doi: 10.1109/ACCESS.2018.2839737.

[4] F. Milano, F. Dörfler, G. Hug, D. J. Hill, and G. Verbic, "Foundations and challenges of low-inertia systems (invited paper)," in *Proc. Power Syst. Comput. Conf. (PSCC)*, Dublin, Ireland, Jun. 2018, pp. 1–25.

[5] L. Vetoshkin and Z. Müller, "A comparative analysis of a power system stability with virtual inertia," *Energies*, vol. 14, no. 11, p. 3277, Jun. 2021.

[6] M. Saeedian, B. Pournazarian, S. S. Seyedalipour, B. Eskandari, and E. Pouresmaeil, "Emulating rotational inertia of synchronous machines by a new control technique in grid-interactive converters," *Sustainability*, vol. 12, no. 13, p. 5346, Jul. 2020, doi: 10.3390/su12135346.

[7] R. Ofir, U. Markovic, P. Aristidou, and G. Hug, "Droop vs. virtual inertia: Comparison from the perspective of converter operation mode," in *Proc. IEEE Int. Energy Conf. (ENERGYCON)*, Jun. 2018, pp. 1–6, doi: 10.1109/ENERGYCON.2018.8398752.

[8] J. Xiao, Y. Jia, B. Jia, Z. Li, Y. Pan, and Y. Wang, "An inertial droop control based on comparisons between virtual synchronous generator and droop control in inverter-based distributed generators," *Energy Rep.*, vol. 6, pp. 104–112, Dec. 2020, doi: 10.1016/j.egyr.2020.12.003.

[9] N. G. Hingorani and L. Gyugyi, "Static shunt compensators: SVC and STATCOM," in *Understanding FACTS: Concepts and Technology of Flexible AC Transmission Systems*. Piscataway, NJ, USA: IEEE Press, 2000, pp. 135–207, doi: 10.1109/9780470546802.ch5.

[10] G. Li, F. Ma, Y. Wang, M. Weng, Z. Chen, and X. Li, "Design and operation analysis of virtual synchronous compensator," *IEEE J. Emerg. Sel. Topics Power Electron.*, vol. 8, no. 4, pp. 3835–3845, Dec. 2020, doi: 10.1109/JESTPE.2019.2943723.

[11] B. K. Poolla, S. Bolognani, and F. Dörfler, "Optimal placement of virtual inertia in power grids," *IEEE Trans. Autom. Control*, vol. 62, no. 12, pp. 6209–6220, Dec. 2017.

[12] F. Calero, C. A. Cañizares, and K. Bhattacharya, "Dynamic modeling of battery energy storage and applications in transmission systems," *IEEE Trans. Smart Grid*, vol. 12, no. 1, pp. 589–598, Jan. 2021, doi: 10.1109/TSG.2020.3016298.

[13] S. Wang, L. Jing, Y. Zhao, H. R. Wickramasinghe, X. Wu, and G. Konstantinou, "Operation of unified power flow controller as virtual synchronous generator," *IEEE Access*, vol. 8, pp. 162569–162580, 2020, doi: 10.1109/ACCESS.2020.3021388.

[14] Markets and Markets. (Aug. 2020). *Flexible AC Transmission Systems (FACTS) Market With COVID-19 Impact Analysis by Compensation Type (Shunt, Series, and Combined), Generation Type, Vertical, Component, Application, Functionality, and Geography—Global Forecast to 2025*. Accessed: Jul. 28, 2021. [Online]. Available: https://www.marketsandmarkets.com/Market-Reports/flexible-ac-transmission-system-market-1228.html

[15] M. Sheppard and S. Saeed. *A Snapshot of Flexible AC Transmission Systems (FACTS) Market in Europe*. Accessed: Jul. 28, 2021. [Online]. Available: https://powertechresearch.com/a-snapshot-of-flexible-ac-transmission-systems-facts-market-in-europe/

[16] *Mathematica*, Version 12.2, Wolfram Res., Champaign, IL, USA, 2020.

[17] P. W. Sauer and M. A. Pai, *Power System Dynamics and Stability*. Upper Saddle River, NJ, USA: Prentice-Hall, 1998.

[18] P. Kundur, *Power System Stability and Control*. New York, NY, USA: McGraw-Hill, 1994.

[19] *IEEE Guide for Synchronous Generator Modeling Practices and Applications in Power System Stability Analyses*, IEEE Standard 1110-2002 (Revision IEEE Standard 1110-1991), Nov. 2003, pp. 1–80, doi: 10.1109/IEEESTD.2003.94408.

[20] E. Brown and G. Weiss, "Using synchronverters for power grid stabilization," in *Proc. IEEE 28th Conv. Electr. Electron. Eng. Israel*, Dec. 2014, pp. 1–5, doi: 10.1109/EEEI.2014.7005736.

[21] H.-D. Chiang, "On-line method for determining power system transient stability," U.S. Patent 5 483 462 A, Jan. 9, 1996.

[22] Q.-C. Zhong, P.-L. Nguyen, Z. Ma, and W. Sheng, "Self-synchronized synchronverters: Inverters without a dedicated synchronization unit," *IEEE Trans. Power Electron.*, vol. 29, no. 2, pp. 617–630, Feb. 2014.

[23] L. Vetoshkin and Z. Müller, "A comparative study of synchronverter stability," in *Proc. 21st Int. Sci. Conf. Electr. Power Eng. (EPE)*, Prague, Czech Republic, Oct. 2020, pp. 1–6.

[24] L. Vetoshkin and Z. Müller, "A supervisory MPC for synchronverter," in *Proc. 21st Int. Sci. Conf. Electr. Power Eng. (EPE)*, Prague, Czech Republic, Oct. 2020, pp. 1–6.

[25] L. Papangelis, M.-S. Debry, T. Prevost, P. Panciatici, and T. Van Cutsem, "Stability of a voltage source converter subject to decrease of short-circuit capacity: A case study," in *Proc. Power Syst. Comput. Conf. (PSCC)*, Dublin, Ireland, Jun. 2018, pp. 1–7.

[26] M. H. Haque and P. Kumkratug, "Application of Lyapunov stability criterion to determine the control strategy of a STATCOM," *IEE Proc., Gener., Transmiss. Distrib.*, vol. 151, no. 3, pp. 415–420, May 2004.

[27] K. R. Padiyar, *Power System Dynamics: Stability and Control*. Anshan, China: Anshan Limited, 2004.

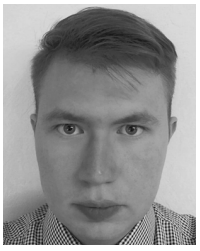

LAVR VETOSHKIN (Member, IEEE) was born in Tyumen, Russia, in 1995. He received the bachelor's degree in applied electrical engineering from Czech Technical University (CTU), Prague, Czech Republic, in 2016, and the master's degree in electrical power engineering, in 2018. He is currently pursuing the Ph.D. degree in electrical power engineering at his alma mater.

ZDENĚK MÜLLER (Senior Member, IEEE) received the Ph.D. degree in electrical engineering from Czech Technical University (CTU), Prague, Czech Republic, in 2012. He has been an Associate Professor at CTU, since 2015. His research interests include intelligent systems for safe and reliable electrical energy supply in power systems, local automation in transmission systems, mitigation of negative effects of nonlinear dynamic loads, smart grid architecture, optimization of protection systems, and applications of WAMS in transmission systems. He is a Senior Member of IEEE PES.